Research Article | Vol. 30, No. 11 / 23 May 2022 / Optics Express 18079
Optics EXPRESS

Optimized multilayer structure for sensitive THz characterization of thin-film glucose solutions

XUEFEI DING,[1] A. I. HERNANDEZ-SERRANO,[1] HANNAH LINDLEY-HATCHER,[1] RAYKO I. STANTCHEV,[1] JUN ZHOU,[2] AND EMMA PICKWELL-MACPHERSON[1,*]

[1]Department of Physics, University of Warwick, Gibbet Hill Road, Coventry, CV4 7AL, UK
[2]Terahertz Research Centre, School of Electronic Science and Engineering, University of Electronic Science and Technology of China, 610054, Chengdu, China
[*]e.macpherson@warwick.ac.uk

Abstract: Terahertz time-domain spectroscopy (THz-TDS) has shown promise in biomedical sample characterization and high characterization sensitivity is in demand due to the thin-film (TF) feature of the sample. This paper proposes an optimized multilayer structure for sensitive characterization of TF aqueous solutions in reflection THz-TDS. Theoretical simulations are conducted for structural optimization and the 75 μm window-sample-mirror structure displays the best sensitivity compared to other sandwich structures and traditional THz measurement geometries. 0-20% TF glucose solutions are then measured; and a spectral peak introduced by the proposed structure is observed to result in the high sensitivity. Our work provides a new way of customizing multilayer structure for THz thin-film characterization.

1. Introduction

Terahertz time-domain spectroscopy (THz-TDS) is a cutting-edge characterization technique that has many potential areas of application [1]. Due to its high water-sensitivity and non-ionizing photon energies, THz-TDS has been widely used in biomedical research [2]. Biomedical samples, including biological solutions and paraffin-embedded tissues, are often small in volume or thickness leading to high requirements on the characterization sensitivity. This is further compounded by the long THz wavelengths [3 mm – 300 μm], when compared to visible light, because what is an optically thick sample is likely to be considered a thin-film (TF) sample for THz frequencies. In TF samples the sample thickness is comparable or smaller than the wavelength which results in very short interaction length between the sample and electromagnetic wave. For time-domain pulsed measurements there is an overlap between pulses during sample measurement resulting in reduced characterization sensitivity. This problem can be alleviated by either reducing system noise or improving the signal contrast induced by the TF sample [3].

Transmission THz-TDS is normally used to measure solid TF samples, however conductive samples can be difficult to characterize accurately because of the significant absorption of THz signal amplitude and the negligible phase shift [4,5]. Attenuated total reflection (ATR) spectroscopy is an efficient way to measure liquid samples, but it requires the sample thickness to be larger than the THz penetration depth which can be hundreds of microns [6,7]. Metamaterial sensing can be used to trace little concentration changes in liquid TF samples, however the fabrication process is often complex and uneconomical [8,9]. Some researchers have been trying to utilize microfluidic techniques for TF liquid measurements [10–13], where the liquid flows through a micro-sized channel whilst being measured by THz waves; and others like Soltani et al. have been researching on manufacturing small-volume liquid sensor based on

#451633 https://doi.org/10.1364/OE.451633
Journal © 2022 Received 19 Dec 2021; revised 17 Feb 2022; accepted 20 Feb 2022; published 10 May 2022

Optics EXPRESS

electromagnetic resonance [14]. Finally, Sun et al. proposed a multilayer structure to enhance the THz characterization sensitivity of aqueous solutions and also paraffin-embedded tissues [15].

Glucose is an essential monosaccharide in the human body and using THz-TDS to study aqueous glucose solutions has aroused researchers' interest [16–18]. Furthermore, with the increasing number of diabetics, methods for blood glucose monitoring have been developed, including vibrational spectroscopic techniques like Raman spectroscopy, mid-infrared and near-infrared spectroscopy [19,20]. In recent years, THz-TDS has been demonstrated to be a powerful tool in measuring diabetic blood plasma ex vivo, and correlations have been seen between the optical properties and blood glucose concentration [21–23]. The aforementioned research has been conducted in bulk reflection geometry or transmission geometry; the former geometry requires large amount of liquid sample and the latter geometry can hardly detect any subtle concentration changes in TF solutions. To measure blood plasma more sensitively without strong THz absorption from water, Lykina et al. pretreated the human blood plasma samples by lyophilization and pressing the powder into pellets before measuring with transmission THz-TDS, however the pretreatment process can be time-consuming and solid-state plasma pellets may have different features compared with real liquid plasma [24].

To overcome the problems outlined above, this paper proposes an optimized multilayer structure to improve the sensitivity of THz characterization of TF glucose solutions with a reflection measurement geometry. In the multilayer structure, the TF liquid sample is sandwiched between a top substrate and an imaging window with a fixed slot thickness. Theoretical simulations are carried out for structural optimization, and we find the most sensitive multilayer structure customized for our samples. TF glucose solutions with different concentrations are then measured, and we show that the signal contrast between different glucose concentrations is enhanced with the proposed structure compared to an ordinary transmission geometry. Our work provides a new method for characterizing TF samples, and results presented here can be used as a reference for future research on THz sensing of blood glucose.

2. Methodology

2.1. Extracting the dielectric properties of thin-film samples

When a TF sample is measured in reflection THz-TDS, the sample is placed on an imaging window, and an additional top substrate could be put on top of the sample and thus form a sandwich structure. In this case, unlike the reflection geometry for bulk sample measurements, the multiple internal reflections inside the TF sample must be considered. As illustrated in Fig. 1, when the THz light is directed onto a TF (Medium 2) there are reflections from both interfaces between the sample and the substrates, therefore the measured reflected and transmitted responses from the structure contain all the reflections from within the TF layer (Fabry-Perot reflections) [25,26].

Thus, the reflection coefficient of such a tri-layer TF geometry is acquired through the summation of the internal reflections. The theoretical sample-reference ratio of geometries commonly used in THz characterization of TF liquid samples are given [27–29]:

$$M_{trans} = \frac{T_{sam}}{T_{ref}} = \frac{t_{sub1-sam-sub2}}{t_{sub1-air-sub2}} = \frac{t_{sub1-sam}t_{sam-sub2}P_{sam}(d_{sam})(1 + r_{sub1-air}r_{air-sub2}P^2_{air}(d_{air}))}{t_{sub1-air}t_{air-sub2}P_{air}(d_{air})(1 + r_{sub1-sam}r_{sam-sub2}P^2_{sam}(d_{sam}))} \tag{1}$$

$$\begin{aligned} M_{TF} &= \frac{R_{sam}}{R_{ref}} = \frac{r_{win-sam-top}}{r_{win-air-top}} \\ &= \frac{(r_{win-sam} + r_{sam-top}P^2_{sam}(d_{sam}\cos\theta_{sam}))(1 + r_{win-air}r_{air-top}P^2_{air}(d_{air}\cos\theta_{air}))}{(1 + r_{win-sam}r_{sam-top}P^2_{sam}(d_{sam}\cos\theta_{sam}))(r_{win-air} + r_{air-top}P^2_{air}(d_{air}\cos\theta_{air}))} \end{aligned} \tag{2}$$

Optics EXPRESS

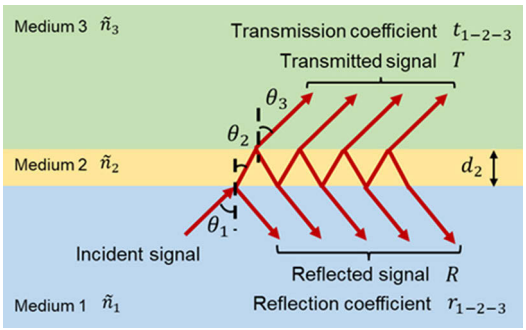

Fig. 1. A schematic diagram of the numerical treatment for thin-film sample (medium 2) in reflection geometry, d_2 is the TF thickness.

$$M_{br} = \frac{R_{sam}}{R_{ref}} = \frac{r_{win-sam}}{r_{win-air}} \tag{3}$$

where M_{trans} is the ratio of the TF liquid measured in transmission geometry, and the sample is sandwiched between two substrates. T_{sam} and T_{ref} are the transmitted signals from the sample and reference, respectively, where the reference is taken with air as "Medium 2" in the middle layer. d_{sam} and d_{air} are the thicknesses of the middle layer for sample and reference. The written form of t_{1-2-3} and r_{1-2-3} represent the transmission and reflection coefficient of a tri-layer TF geometry formed by "Medium 1", "Medium 2" and "Medium 3" sequentially; t_{1-2} and r_{1-2} represent the transmission and reflection coefficients from "Medium 1" to "Medium 2". $P_2(d_2) = \exp(-i\omega\tilde{n}_2 d_2/c)$ is the phase propagation and amplitude attenuation in "Medium 2" for a distance of d_2, and $\tilde{n}_2 = n_2 - ik_2$ is the complex refractive index. The subscripts "sub1", "sub2", "sam" and "air" stand for substrate 1, substrate 2, sample and air respectively. Similarly, M_{TF} is the ratio of the TF liquid measured in a tri-layer reflection geometry, where the sample is sandwiched by an imaging window (subscript "win") on the bottom and a top substrate (subscript "top"). R_{sam} and R_{ref} represent the sample and reference signal, and reference would be the reflected signal from this tri-layer system with air as "Medium 2". θ_{sam} and θ_{air} are the refractive angles in the middle layer of the sample and air respectively. Finally, M_{br} is the ratio of bulk sample measured in reflection geometry, where sample would be placed on an imaging window; the reference signal is taken using the bare window.

2.2. THz characterization sensitivity

In THz material characterization, the optical properties of a sample can be extracted by fitting the experimentally measured sample-reference ratio to the theoretically calculated ratio M (Eqs. (1–3)). When measuring a group of samples with similar optical properties, the values of M are often close for every sample, leading to systematic errors in the classification of those samples. Therefore, measurement geometries that can produce larger differences between the sample-reference ratios have higher sensitivities in measuring such samples. Thus the characterization sensitivity of a geometry can be defined by the relative change rate (RC) of M

$$RC_{abs(M)} = \left| \frac{abs(M) - abs(M_{0\%})}{abs(M_{0\%})} \times 100\% \right| \tag{4}$$

where $M_{0\%}$ is the base value by definition (i.e., when measuring aqueous solution samples with different concentrations, it can be the theoretical ratio of pure water).

Optics EXPRESS

2.3. Optimization of the multilayer structure

Sun et al. proposed a prism-sample-quartz tri-layer sandwich structure and utilized it to characterize aqueous ethanol solutions [15]. We further investigate into this idea by considering the top substrate refractive index and the slot thickness of the sandwich structure as two variables and optimize them to find out the most sensitive structure, in other words it has the largest relative change in M for the samples to be measured. Here, the samples are aqueous glucose solutions (Glu-Sols) with different mass fractions. Simulations are conducted in MATLAB by calculating Eq. (1), and the theoretical complex refractive indices of the mixtures are estimated by Landau-Liftshitz-Looyenga Effective Medium Theory [30].

The top substrates are categorized into four types according to their refractive index (n) relative to that of the imaging window (made of quartz, $n_{win} = 2.1$), and the ratio is defined as $N = n/n_{win}$. The slot thickness is varied in the range of 25-75 μm which is below the wavelength of 1 THz. As shown in Fig. 2(a-b), when the top substrate has a smaller (N<1) or similar ($N \approx 1$) refractive index to the window, the curve of relative change in abs(M) has a steeper rise as the slot thickness d decreases, and thus the structure is most sensitive when $d = 25$μm. The high sensitivity comes from the matching the impedance of the top and bottom layer, therefore a thinner sample layer produces higher sensitivity. While in Fig. 2 (c-d), when the top substrate has a larger (N>1) or far larger ($N \gg 1$) refractive index, there is an opposite trend as the $RC_{abs(M)}$ curve grows steeper when the slot thickness increases, and then reaches the highest slope at $d = 75$μm. Here we suppose the high sensitivity is related to the addition of pulses reflected from the lower and upper interface of sample, and when the slot thickness increases to a certain value, the overlapping between pulses introduces high contrast in M.

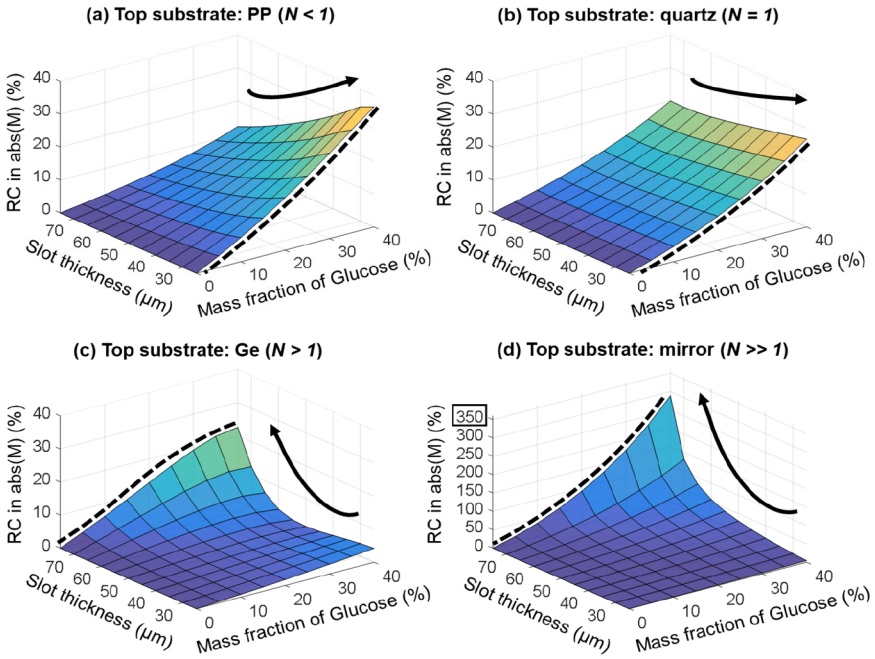

Fig. 2. Simulation of the $RC_{abs(M)}$ for different 'sandwich' structures at 0.6 THz: (a) top substrate: polypropylene (PP, $n = 1.5$, N<1) [31], slot thickness: 25-75 μm; (b) top substrate: quartz ($n = 2.1$, $N \approx 1$), slot thickness: 25-75 μm; (c) top substrate: Germanium (Ge, $n = 4$, N>1.) [32], slot thickness: 25-75 μm; (d) top substrate: mirror (assumed to have the same refractive index as highly-reflective metal, $n = 300$, N>1) [33], slot thickness: 25-75 μm.

Optics EXPRESS

Altogether, Fig. 2 shows that the sandwich structure with mirror as the top substrate and 75 μm slot thickness displays the most significant contrast in THz responsivity as the Glu-Sol concentration changes. The new 75 μm window-sample-mirror (win-sam-mirr) structure is then compared with the 25 μm prism-sample-quartz (psm-sam-qz) structure proposed in [15]. Figure 3 displays the $RC_{abs(M)}$ for different THz measurement geometries at 0.5, 0.6, 0.7 THz, including sandwich structures in reflection geometry: 75 μm window-sample-mirror (refle, win-sam-mirr), 75 μm prism-sample-mirror (refle, psm-sam-mirr), 25 μm window-sample-quartz (refle, win-sam-qz), 25 μm prism-sample-quartz (refle, psm-sam-qz); and ordinary bulk reflection geometry (bulk refle) and transmission geometry with 75 μm thickness (trans). The figure indicates that the 75 μm win-sam-mirr structure has the largest variation in $RC_{abs(M)}$ with gradient approximately 3 times of other geometries at 0.5 THz and 10 times of others at 0.6 and 0.7 THz. Simulations have also been conducted at other frequency points and the 75 μm win-sam-mirr structure gives better sensitivity in the range of 0.4-0.8 THz.

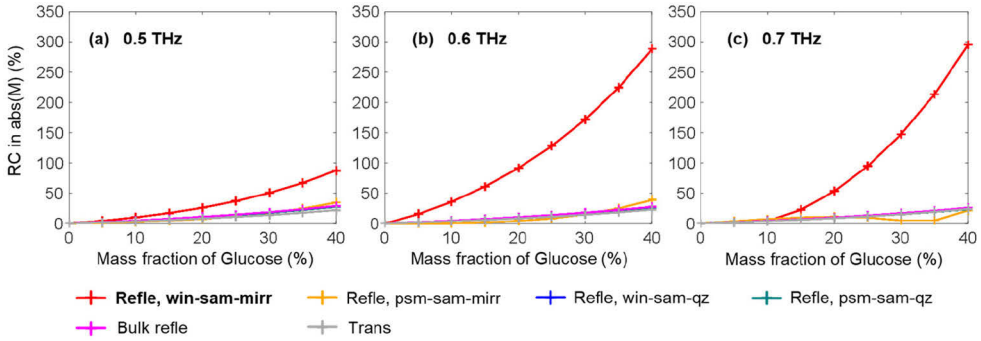

Fig. 3. Comparison of the $RC_{abs(M)}$ for different THz measurement geometries at 0.5, 0.6, 0.7 THz.

2.4. Experimental setup and protocol

In this study, a TeraView TPS spectra 3000 spectrometer was used for measurements; for reflection geometry, the incident angle is 45°, and the incident THz wave is s-polarized. Figure 4 shows the design of the 75 μm win-sam-mirr structure, where the top substrate is a silver-plated reflecting mirror, the bottom substrate is the quartz imaging window from the THz system, and they are spaced by two 75 μm thick Teflon spacers. Glu-Sol samples with mass fraction in the range of 0-20% at 5% intervals (Δ = 5%) were made from dehydrated D-glucose powder (Fisher Chemical) and distilled water; Glu-Sol concentrations up to 20% were chosen for experiments due to the practicality of sample preparation and storage. Higher glucose concentrations could be used but they are more difficult to prepare. The technique could also be extended to measure other solutions including protein solutions.

For the experimental procedure of the win-sam-mirr structure, we started with the acquisition of the slot thickness, which is a crucial step for the subsequent properties extraction process. First we measured the window-air interface (win-air) of the bare imaging window as a reference signal (ref1); then we placed spacers, quartz and a weight sequentially to form a window-air-quartz structure (win-air-qz) and acquired the reflected signal from the middle layer as a sample signal (sam1); and eventually by fitting the experimental ratio R_{sam1}/R_{ref1} to the theoretical ratio, we could get the slot thickness. We use win-air-qz instead of win-air-mirr for thickness acquisition is because the former structure is more sensitive to the change in slot thickness. Here the combination of the spacers and weight is for thickness control, so that we would not expect any change in the slot thickness during the measurements of different samples.

Optics EXPRESS

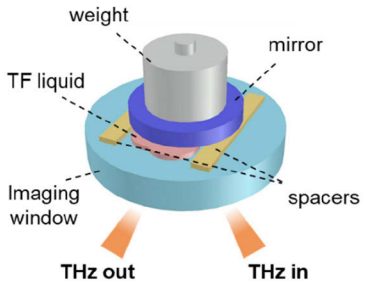

Fig. 4. A schematic diagram of the win-sam-mirr structure.

In the sample measurement process, we replaced the top substrate quartz with a mirror and used the reflected signal from the window-air-mirror structure (win-air-mirr) as reference (ref2). Then after taking away the weight and mirror, we dropped an appropriate amount of the aqueous sample on the imaging window, placed the mirror and weight on again, and then finally measured the window-sample-mirror layer (win-sam-mirr) as our sample signal (sam2). Optical properties of the sample are then extracted by fitting the experimental ratio R_{sam2}/R_{ref2} to the theoretical ratio as given in Eq. (2).

Measurements are also conducted in bulk reflection and transmission geometries: for the former geometry, bulk liquid is held within a 2.5 mm-thick polymer ring placed on the imaging window; for the latter geometry, a liquid sample cell with two polymer wafers (n = 1.454) and a 75 μm Teflon spacer is used to hold the liquid.

3. Results and discussion

3.1. Validation of the proposed geometry

We first measured TF water in the proposed win-sam-mirr structure in order to validate the results, the extracted optical properties were compared with those measured in bulk reflection and transmission geometries and also the results from references [34,35]. As shown in Fig. 5, the refractive index and absorption coefficient match well with the results from other geometries and references. Some variation between the literature values comes from differences in the experimental environment and system, while results from win-sam-mirr and transmission agree within 2%. The error bars on the win-sam-mirr results are the standard deviation from 3 repeat measurements and the narrow span shows good robustness and repeatability.

3.2. Measurements of Glu-Sols with different concentrations

Glu-Sol samples with concentrations in the range of 0-20% at 5% intervals were measured with the 75 μm win-sam-mirr structure; and samples with 0, 10% and 20% concentrations were measured with transmission geometry for comparison. Figure 6(a-b) show the THz time-domain signals measured with the win-sam-mirr and transmission geometries respectively; where the reference pulses have been multiplied by a factor of 0.3 and 0.5 respectively. In the results from the win-sam-mirr structure, there is an overlap of multiple reflected THz pulses which creates a notable peak distinguishing different Glu-Sols as shown in Fig. 6(a). Figure 6(c) shows the frequency-domain signals of both geometries, which are obtained by performing the Fast Fourier Transform (FFT) on the time domain signals. A peak is also visible in the win-sam-mirr signals at 0.6-0.7 THz, leading to high contrast in the experimental sample over reference ratios of different Glu-Sols as shown in Fig. 6(e). The shape of each resonance is related to the refractive index of the liquid sample. In particular, the depth of the resonance is related to the Fresnel coefficients, and the frequency position is related to the relative delay between the echoes. Figure 6(d)

Optics EXPRESS

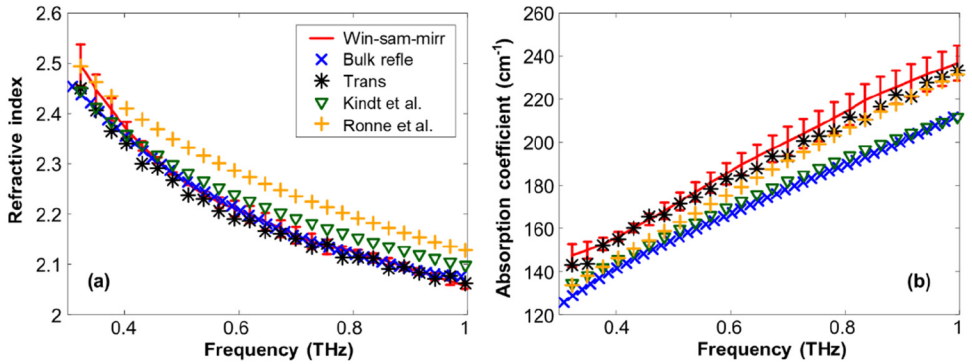

Fig. 5. (a) The refractive index and (b) absorption coefficients of water measured with the win-sam-mirr structure and the bulk reflection and transmission geometries, compared to literature results [34,35].

illustrates the relative change in FFT integral as glucose concentration increases from 0% to 20%; due to the introduced peak, the change in the FFT integral of the win-sam-mirr signals is much larger compared to the transmission signals, with the gradient approximately 5 times of the latter.

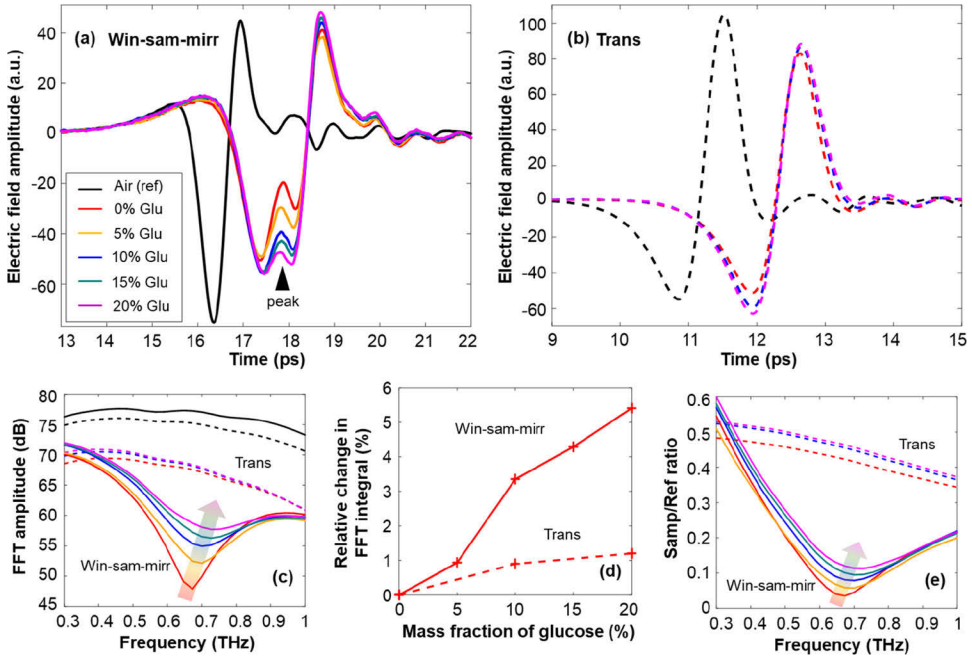

Fig. 6. (a) THz time-domain signals of 0~20% Glu-Sols (Δ = 5%) measured using the win-sam-mirr structure; reference signal is shifted and shrunk by 0.3x for clear display; (b) THz time-domain signals of 0~20% Glu-Sols (Δ = 10%) measured using the transmission geometry; reference signal is shifted and shrunk by 0.5x for clear display; (c) THz frequency-domain signals of Glu-Sols measured by both geometries; (d) the correlation of relative change in FFT integral and glucose concentration; (e) experimental ratio of Glu-Sols measured by both geometries.

Compared to the results acquired by transmission geometry, the win-sam-mirr structure has a better capability for enhancing the contrast between different concentrations of Glu-Sol samples

Optics EXPRESS

by introducing a notable peak in both the time- and frequency-domain signals. The relative change in the experimental ratio of Glu-Sols measured by win-sam-mirr is also enlarged around the peak, which agrees with the large variation in $RC_{abs(M)}$ in the previous simulation results.

Using the slot thickness acquired in the previous process, the optical properties of the Glu-Sol samples measured with the win-sam-mirr structure were extracted and compared to those extracted from measurements performed in the transmission geometry. As illustrated in Fig. 7, the refractive indices and absorption coefficients measured by both geometries match well for Glu-Sols with 10% concentration difference. Furthermore, the proposed win-sam-mirr structure can reliably detect samples with 5% concentration difference: this is below the sensitivity that can be reliably detected using transmission geometry. In Fig. 7(a), refractive indices of Glu-Sols with 5% concentration difference are close to each other, yet they can still be clearly distinguished in the range of 0.3-0.5 THz without the error bars overlapping (as shown in the inset figure). In Fig. 7(b), the absorption coefficients of different Glu-Sols measured using the sandwich structure are distinguishable throughout the measured frequency range with no overlapping of error bars for most frequencies. However, in transmission geometry, the error bars are much larger and as seen in the inset of Fig. 7(b), they already start to overlap in the range 0.3-0.5 THz even when the change in concentration is 10%. This highlights the lower sensitivity achievable in transmission geometry.

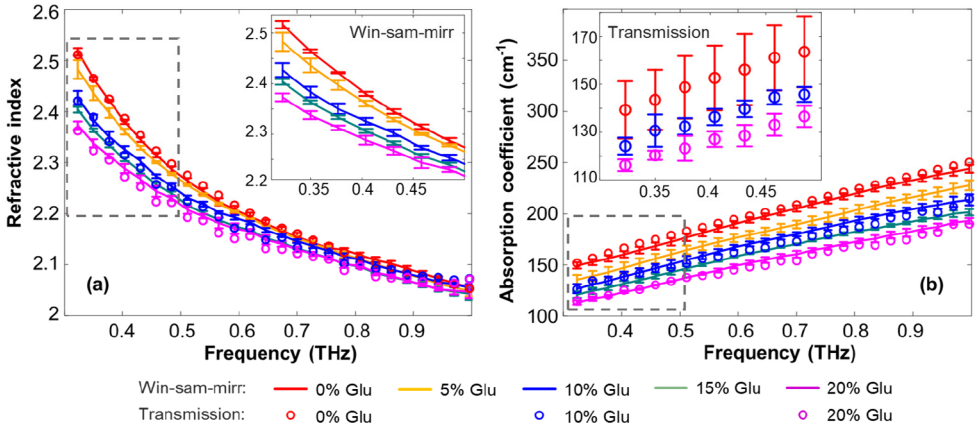

Fig. 7. (a) The refractive indices and (b) absorption coefficients of 0~20% Glu-Sols measured by win-sam-mirr structure and transmission geometry. The inset in (a) shows the error bars for the win-sam-mirr structure. The inset in (b) shows the error bars for the transmission data. The error bars are the standard deviation from three measurements.

Figure 8 plots the correlation between the optical properties and glucose concentration. The refractive index and absorption coefficient of Glu-Sols are reported to have a linear relationship with the concentration of the solute, so a first order polynomial is fitted to each of the experimental data curves [35,36]. The fitted polynomials and the Pearson correlation coefficients r are annotated in the figures. In general, a decreasing trend can be seen in both the refractive index and absorption coefficient, and according to the correlation coefficients, both properties show very strong linear correlation with the mass fraction of glucose with $|r|>0.98$ for all the three frequencies. For refractive index, the slope of the fitted lines decreases as the frequency increases from 0.3 THz to 0.5 THz, and the change rate of the refractive index is 30%, 47% and 73% per percentage concentration for 0.3, 0.4 and 0.5 THz; whereas for absorption coefficient the slope increases with frequency, and the change rate is between 174%, 177% and 190% per percentage concentration for 0.3, 0.4 and 0.5 THz. The correlation between the optical properties and the

Optics EXPRESS

solute concentration shows potential in estimating the concentration of an unknown Glu-Sol by measuring its refractive index and/or absorption coefficient.

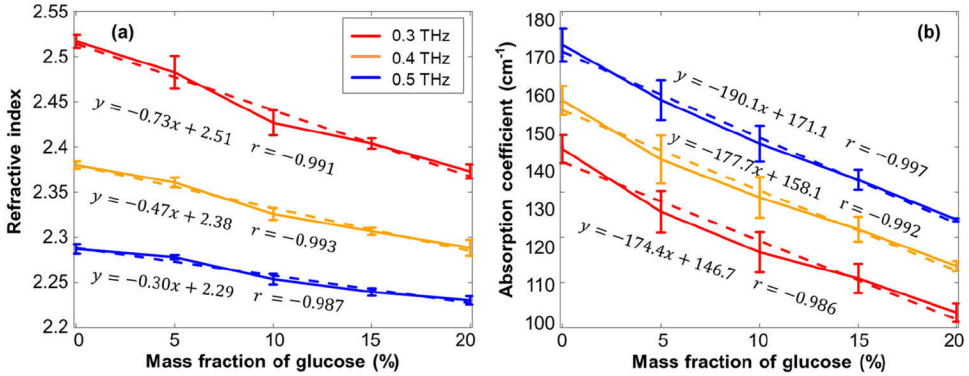

Fig. 8. The correlation of (a) refractive index, (b) absorption coefficients and glucose concentration at 0.3 THz, 0.4 THz and 0.5 THz measured by win-sam-mirr structure. Dashed lines are the first order polynomials fitted to the experimental data; *r* is the Pearson correlation coefficient.

Glu-Sols with mass fraction of 0~20% contain a high proportion of water, and the 5% concentration difference leads to small differences in the refractive indices; hence, limited by the experimental system, sensitive characterization of Glu-Sols could be difficult, while absorption coefficients are more acquirable than refractive indices. The peak in THz time- and frequency-domain signals introduced by our geometry could be used in the application of THz sensing of Glu-Sols with little concentration differences, and the linear correlation between the optical properties and the glucose concentration could be used in mapping Glu-Sol concentration to our THz-TDS technique.

4. Summary

In this work, we propose an optimized sandwich structure (75 μm win-sam-mirr) for sensitive THz characterization of thin-film aqueous glucose solutions. We conduct theoretical simulations to quantify the characterization sensitivity of the sandwich structure with different top substrates and slot thicknesses, and compare the sensitivity of our proposed structure with other THz geometries to show its advantage in thin-film characterization. We then utilize the proposed win-sam-mirr structure to measure thin-film liquids; thin-film water is measured for validation, and thin-film Glu-Sols with mass fractions between 0% and 20% are measured. The results are compared to those acquired by the ordinary transmission geometry. A notable peak is observed in both time- and frequency-domain signals, which is introduced by the use of our proposed geometry and enhances the contrast between the sample-reference ratios of different Glu-Sols. Experimental results are in line with the theoretical simulations and indicate that the high sensitivity comes from the overlapping effect of multiple reflected THz signals. Optical properties of 0~20% Glu-Sols are also extracted and linear correlation is found between the refractive index, absorption coefficient and glucose concentration. Our work provides a new train of thought for THz thin-film characterization: with the proposed approach of utilizing theoretical simulation to optimize multilayer structures, such a structure could be customized for sensitive measurements of specific thin-film samples. The observed spectral feature at 0.6-0.7 THz introduced by our structure shows potential in THz sensing of Glu-Sols.

Funding. China Scholarship Council (Xuefei Ding); Royal Society (Merit Award); Engineering and Physical Sciences Research Council (EP/S021442/1).

Optics EXPRESS

Disclosures. The authors declare no conflicts of interest.

Data availability. Data underlying the results presented in this paper are available in Ref. [37].

References

1. A. Irizawa, S. Lupi, and A. J. C. M. Marcelli, "Terahertz as a Frontier Area for Science and Technology," Condensed Matter **6**(3), 23 (2021).
2. A. Gong, Y. Qiu, X. Chen, Z. Zhao, L. Xia, and Y. Shao, "Biomedical applications of terahertz technology," Appl. Spectrosc. Rev. **55**(5), 418–438 (2020).
3. J. F. O'Hara, W. Withayachumnankul, and I. Al-Naib, "A review on thin-film sensing with terahertz waves," J. Infrared, Millimeter, Terahertz Waves **33**(3), 245–291 (2012).
4. M. Mumtaz, M. A. Mahmood, R. Rashid, M. Ahmed, M. A. Zia, and I. J. L. P. L. Ahmad, "Investigation of the optical and conductive properties of antimony-doped titanium dioxide using terahertz time-domain spectroscopy," Laser Phys. Lett. **15**(10), 105603 (2018).
5. X. Liu, E. P. Parrott, B. S.-Y. Ung, and E. Pickwell-MacPherson, "Exploiting total internal reflection geometry for efficient optical modulation of terahertz light," APL Photonics **1**(7), 076103 (2016).
6. H. Hirori, K. Yamashita, M. Nagai, and K. J. J. J. O. A. P. Tanaka, "Attenuated total reflection spectroscopy in time domain using terahertz coherent pulses," Jpn. J. Appl. Phys. **43**(No. 10A), L1287 (2004).
7. M. Nagai, H. Yada, T. Arikawa, and K. Tanaka, "Terahertz time-domain attenuated total reflection spectroscopy in water and biological solution," Int. J. Infrared Millimeter Waves **27**(4), 505–515 (2007).
8. D.-K. Lee, J.-H. Kang, J.-S. Lee, H.-S. Kim, C. Kim, J. Hun Kim, T. Lee, J.-H. Son, Q. H. Park, and M. Seo, "Highly sensitive and selective sugar detection by terahertz nano-antennas," Sci. Rep. **5**(1), 15459 (2015).
9. Y. Roh, S.-H. Lee, B. Kang, J. W. Wu, B.-K. Ju, and M. Seo, "Terahertz optical characteristics of two types of metamaterials for molecule sensing," Opt. Express **27**(13), 19042–19049 (2019).
10. L. Chen, D.-G. Liao, X.-G. Guo, J.-Y. Zhao, Y.-M. Zhu, and S.-L. Zhuang, "Terahertz time-domain spectroscopy and micro-cavity components for probing samples: a review," Frontiers Inf Technol Electronic Eng **20**(5), 591–607 (2019).
11. M. Tonouchi, "Terahertz microfluidic chip sensitivity-enhanced with a few arrays of meta atoms," in *Optical Sensors*, (Optical Society of America, 2018), SeTh4E. 1.
12. R. Zhang, Q. Chen, K. Liu, Z. Chen, K. Li, X. Zhang, J. Xu, and E. Pickwell-MacPherson, "Terahertz Microfluidic Metamaterial Biosensor for Sensitive Detection of Small-Volume Liquid Samples," IEEE Trans. Terahertz Sci. Technol. **9**(2), 209–214 (2019).
13. X. Ding, J. Zhou, and E. Pickwell-MacPherson, "Optimized multilayer structure for sensitive THz characterization of thin-film aqueous solutions," in *2021 46th International Conference on Infrared, Millimeter and Terahertz Waves (IRMMW-THz)*, (IEEE, 2021), 1–2.
14. A. Soltani, H. Neshasteh, A. Mataji-Kojouri, N. Born, E. Castro-Camus, M. Shahabadi, and M. Koch, "Highly sensitive terahertz dielectric sensor for small-volume liquid samples," Appl. Phys. Lett. **108**(19), 191105 (2016).
15. Q. Sun, K. Liu, X. Chen, X. Liu, A. Hernandez-Serrano, and E. Pickwell-MacPherson, "Utilizing multilayer structures to enhance terahertz characterization of thin films ranging from aqueous solutions to histology slides," Opt. Lett. **44**(9), 2149–2152 (2019).
16. C. Song, W.-H. Fan, L. Ding, X. Chen, Z.-Y. Chen, and K. Wang, "Terahertz and infrared characteristic absorption spectra of aqueous glucose and fructose solutions," Sci. Rep. **8**(1), 8964 (2018).
17. Z.-F. Jiang, Y.-X. Wang, X.-H. Li, C.-Z. Lu, W. Liu, P. Sun, and L. Miao, "Terahertz time-domain spectroscopy of D-glucose in the solution states," in *International Symposium on Photoelectronic Detection and Imaging 2013: Imaging Spectrometer Technologies and Applications*, (International Society for Optics and Photonics, 2013), 89101 T.
18. P. U. Jepsen, U. Møller, and H. Merbold, "Investigation of aqueous alcohol and sugar solutions with reflection terahertz time-domain spectroscopy," Opt. Express **15**(22), 14717–14737 (2007).
19. S. Delbeck, T. Vahlsing, S. Leonhardt, G. Steiner, and H. M. Heise, "Non-invasive monitoring of blood glucose using optical methods for skin spectroscopy—opportunities and recent advances," Anal. Bioanal. Chem. **411**(1), 63–77 (2019).
20. W. Villena Gonzales, A. T. Mobashsher, and A. Abbosh, "The progress of glucose monitoring—A review of invasive to minimally and non-invasive techniques, devices and sensors," Sensors **19**(4), 800 (2019).
21. H. Chen, X. Chen, S. Ma, X. Wu, W. Yang, W. Zhang, and X. Li, "Quantify Glucose Level in Freshly Diabetic's Blood by Terahertz Time-Domain Spectroscopy," J. Infrared, Millimeter, Terahertz Waves **39**(4), 399–408 (2018).
22. D. Wang, Y. Zhang, J. Han, X. Li, X. Chen, T. Qiu, and H. Chen, "Quantification of triglyceride levels in fresh human blood by terahertz time-domain spectroscopy," Sci. Rep. **11**(1), 13209 (2021).
23. M. R. Konnikova, O. P. Cherkasova, M. M. Nazarov, D. A. Vrazhnov, Y. V. Kistenev, S. E. Titov, E. V. Kopeikina, S. P. Shevchenko, and A. P. Shkurinov, "Magnant and benign thyroid nodule differentiation through the analysis of blood plasma with terahertz spectroscopy," Biomed. Opt. Express **12**(2), 1020–1035 (2021).
24. A. L. Anastasia, M. N. Maxim, R. K. Maria, A. M. Ilia, L. V. Vladimir, A. A. Vladimir, G. D. Elena, B. C. Mariya, V. K. Yury, A. V. Denis, V. P. Vladimir, A. K. Yulia, V. K. Dmitry, P. C. Olga, P. S. Alexander, Y. B. Alina, and A. S. Olga, "Terahertz spectroscopy of diabetic and non-diabetic human blood plasma pellets," J. Biomed. Opt. **26**, 043006 (2021).

Optics EXPRESS

25. C. Fabry, "Theorie et applications d'une nouvelle methods de spectroscopie intereferentielle," Ann. Chim. Ser. **16**, 115–144 (1899).
26. A. Perot and C. Fabry, "On the application of interference phenomena to the solution of various problems of spectroscopy and metrology," Astrophys. J. **9**, 87 (1899).
27. J. D. E. McIntyre and D. E. Aspnes, "Differential reflection spectroscopy of very thin surface films," Surf. Sci. **24**(2), 417–434 (1971).
28. M. Milosevic, "Internal Reflection and ATR Spectroscopy," Appl. Spectrosc. Rev. **39**(3), 365–384 (2004).
29. X. Chen, E. P. J. Parrott, B. S. Ung, and E. Pickwell-MacPherson, "A Robust Baseline and Reference Modification and Acquisition Algorithm for Accurate THz Imaging," IEEE Trans. Terahertz Sci. Technol. **7**(5), 493–501 (2017).
30. H. Looyenga, "Dielectric constants of heterogeneous mixtures," Physica **31**(3), 401–406 (1965).
31. E. Fedulova, M. Nazarov, A. Angeluts, M. Kitai, V. Sokolov, and A. Shkurinov, "Studying of dielectric properties of polymers in the terahertz frequency range," *Saratov Fall Meeting 2011* (SPIE, 2012), Vol. 8337.
32. M. H. Bergen and J. F. Holzman, "Terahertz Time-Domain Spectroscopy for Ultrafast and Quasi-Static Characterizations of Germanium," IEEE Trans. Terahertz Sci. Technol. **11**(1), 54–61 (2021).
33. S. Wen-Feng, W. Xin-Ke, and Z. Yan, "Measurement of Refractive Index for High Reflectance Materials with Terahertz Time Domain Reflection Spectroscopy," Chin. Phys. Lett. **26**(11), 114210 (2009).
34. C. Ronne, L. Thrane, P. O. Astrand, A. Wallqvist, K. V. Mikkelsen, and S. R. Keiding, "Investigation of the temperature dependence of dielectric relaxation in liquid water by THz reflection spectroscopy and molecular dynamics simulation," J. Chem. Phys. **107**(14), 5319–5331 (1997).
35. J. T. Kindt and C. A. Schmuttenmaer, "Far-Infrared Dielectric Properties of Polar Liquids Probed by Femtosecond Terahertz Pulse Spectroscopy," J. Phys. Chem. **100**(24), 10373–10379 (1996).
36. F. Glover and J. Goulden, "Relationship between refractive index and concentration of solutions," Nature **200**(4912), 1165–1166 (1963).
37. S. Ding, "multilayer structure paper," figshare, (2022), http://doi.org/10.6084/m9.figshare.19191227.v1